Eurographics Symposium on Geometry Processing (2006)
Konrad Polthier, Alla Sheffer (Editors)

A C^2 Polar Jet Subdivision

K. Karčiauskas[0] and A. Myles[1] and J. Peters [†1]

[0] University of Vilnius [1] University of Florida

Abstract

We describe a subdivision scheme that acts on control nodes that each carry a vector of values. Each vector defines partial derivatives, referred to as jets in the following and subdivision computes new jets from old jets. By default, the jets are automatically initialized from a design mesh. While the approach applies more generally, we consider here only a restricted class of design meshes, consisting of extraordinary nodes surrounded by triangles and otherwise quadrilaterals with interior nodes of valence four. This polar mesh structure is appropriate for surfaces with the combinatorial structure of objects of revolution and for high valences.

The resulting surfaces are curvature continuous with good curvature distribution near extraordinary points. Near extraordinary points the surfaces are piecewise polynomial of degree (6,5), away they are standard bicubic splines.

Categories and Subject Descriptors (according to ACM CCS): I.3.5 [Computer Graphics]: Curve, Surface, Solid, and Object Representations

1. Introduction

We present a subdivision algorithm for a restricted class of meshes as depicted in Figure 1. This *polar mesh structure* [KP06b], while very special, is natural for meshes with the combinatorial structure of surfaces of revolution and locally, for many-sided blends and vertices of high valence. Often, for example for reflective surfaces such as inside car headlights, exactly these high-valence blends require good curvature distribution. However, for standard subdivision schemes, high valence leads to visibly poor shape as illustrated in Figure 2.Indeed, standard schemes have been shown to generate saddles even though the initial control net has a convex triangulation [KPR04]. While it is notoriously difficult to argue that a scheme results in high-quality surfaces, or even to define high quality, the proposed scheme does not exhibit the high-valence flaws observed for standard schemes.

Polar jet subdivision has the following properties.
1. Linear, stationary, affine invariant refinement of a control structure.
2. Control nodes of arbitrary valence.
3. Generates *curvature continuous* surfaces that
4. do not have obvious shape limitations for high valence and
5. can be represented as a sequence of polynomial pieces of degree (6,5).

While the user manipulates a *design mesh*, the scheme refines vectors, called *2-jets*, that are associated with nodes. The approach generalizes bi-cubic spline subdivision to a polar mesh. Polar subdivision schemes can be designed to apply few rules with small footprint directly to the design mesh, as in standard subdivision, but such simplicity results in poorer shape and smoothness when compared with the proposed jet subdivision scheme.

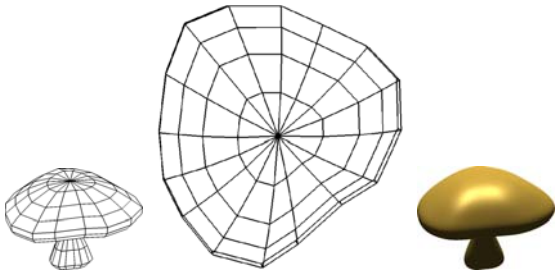

Figure 1: *A polar design mesh: the extraordinary vertex is surrounded by triangles. All quadrilaterals have nodes of valence four.*

† supported by NSF DMI-0400214 and CCF-0430891

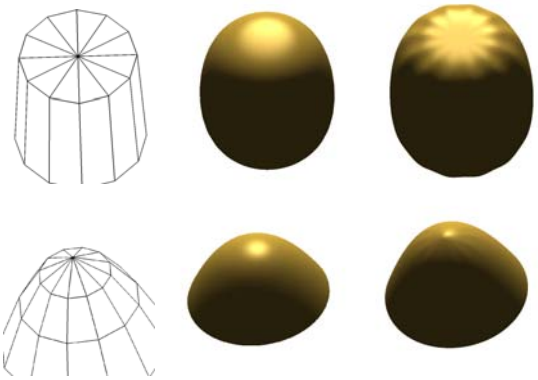

Figure 2: *(left) Polar control net, (middle) polar jet subdivision surface, (right) Catmull-Clark subdivision surface applied to the control net with the central node removed; similar ripples occur near the extraordinary point of the mushroom in Figure 1, also when rendered with Loop's subdivision.*

2. Background

Curvature continuous schemes. A number of piecewise polynomial and even subdivision constructions are known to generate curvature continuous surfaces, for example, as an incomplete listing, [GH89, Pra97, Rei98, Pet02, Loo04]; also a variety of nonpolynomial schemes, based on two Catmull-Clark refinement steps, yield C^2 and even smoother surfaces [CNG00, GH95, YZ04, Lev06]. Due to averaging, shape problems occur in the transition between the 'regular regions' that make up the bulk of the surfaces and the immediate neighborhood of extraordinary points of high valence. Recently, Guided Subdivision [KP06a] suggested a transition by sampling (rather than averaging with) a high-degree spline cap that serves as a shape guide. Polar jet subdivision is inspired by this approach but uses *local jets in place of an explicit guide surface*. This makes the neighborhood of the extraordinary point more responsive to the shape in the adjacent tensor-product region of the surface, and it makes the refinement look more like standard subdivision.

Subdivision surfaces Any of [ZS00, WW02, RP05] give a good introduction to subdivision surfaces. To date no general subdivision algorithm is published that generates everywhere C^2-surfaces without obvious shape deficiencies, restrictions at the extraordinary point or on the overall control net: for example, the scheme [PU98] creates and leverages zero curvature at extraordinary points, [LL03, SW05] join two different subdivision schemes smoothly along edges only and [ZLLT06] creates C^2 subdivision functions with a single extraordinary point and special transitions across edges of the control net. Approaches that associate multiple values and functions with each node, called Hermite or jet subdivision have shown promise in a special case of valence three [XYD06], but do not yet improve the setup at extraordinary points, in general. Tensored circle preserving schemes [MWW01, SD05], double the valence at the poles with each refinement step. In polar subdivision the valence stays fixed.

3. Jet Initialization and Refinement

A *polar design mesh* consists of extraordinary nodes, surrounded by one layer of triangles, and of quadrilaterals with nodes of valence four otherwise (see Figures 1, 2). The extraordinary nodes need only be separated by one layer of nodes of valence four: for example, two pyramids with their polygonal bases joined yield a valid polar design mesh. Quadrilaterals in the input net will be interpreted as part of a standard uniform bicubic B-spline control net (with adjacent triangles viewed as degenerate quadrilaterals). Section 4 explains how bicubic B-spline subdivision can be interpreted as jet subdivision. Triangular facets are, in each subdivision step, split into a smaller triangle attached to the extraordinary node and a quad. The quads form a ring with jets that, in the mth iteration, define a surface ring $\mathbf{x}^m$ (see Figure 3). The bulk of this paper explains how to define and refine the jets associated with the triangular facets.

Figure 3: *A nested sequence of surface rings $\mathbf{x}^1$, $\mathbf{x}^2$, ... converging towards the extraordinary point.*

The actual refinement of jets is hidden from the end user. A designer manipulates a familiar design control mesh, where the nodes have only position. The jets are automatically generated and refined (see Sections 3.2 and 3.3).

3.1. Refinement per sector

The refinement of a subdivision control net can be *localized* by splitting the control net into overlapping, consistently refined subnets. For example, Catmull-Clark subdivision can be localized to subnets consisting of one quadrilateral and its neighbors. For polar jet subdivision, (one coordinate of) the surface corresponding to triangle i is defined by a subnet of four jets (see Figure 4)

$$\mathbf{c}_i^0 \in \mathbb{R}^6,\ \mathbf{v}_i^0 \in \mathbb{R}^9,$$
$$\mathbf{v}_{i+1}^0 \in \mathbb{R}^9,\ \mathbf{e}_i^0 \in \mathbb{R}^3.$$

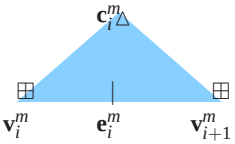

Figure 4: *The four jets forming $\mathbf{j}_i^0$ defining sector i. The icon $\boxplus$ stands for the 3×3 grid of entries $\mathbf{v}_i^0$, the icon $|$ for jets $\mathbf{e}_i^0$ and $\triangle$ for $\mathbf{c}_i^0$.*

As shown in Figure 5, the central jet $\mathbf{c}_i^0$ is represented as

a 'triangular' Bézier mesh of depth two i.e. six entries. We assign the icon △ to this jet as a mnemonic help (see Figure 4). The vertex jets $\mathbf{v}_i^0$ are tensor-degree 2-jets in B-spline form (icon ⊞, compare with Figure 5), i.e. 3×3 entries and the interspersed edge-jets $\mathbf{e}_i^0$ are 2-jets in a single variable in B-spline form, 3 entries, with icon |. That is, we use B-spline representation where possible since Bézier representation is particular to one patch and in that sense unsymmetric. We group the jets into the column vector

$$\mathbf{j}_i^0 := [\mathbf{c}_i^0; \mathbf{v}_i^0; \mathbf{v}_{i+1}^0; \mathbf{e}_i^0] \in \mathbb{R}^{27}.$$

There is one such vector for each x,y,z- coordinate. The sharing of the vertex jets $\mathbf{v}_i^0$ and the relation $\mathbf{c}_{i+1}^m = R\mathbf{c}_i^m$ (R listed in Appendix 6.1), guarantee consistency of the localized computation.

3.2. Initialization of jets from a design mesh

To allow a designer to work with only positional information, we automatically generate the jets $\mathbf{j}_i^0$ from a *design control mesh* $\mathbf{d}$. Let $\mathbf{d}_0$ be the position of the extraordinary node, $\mathbf{d}_1,\ldots,\mathbf{d}_N$ the 1-link (1-ring) of direct neighbors and $\mathbf{d}_{N+1},\ldots,\mathbf{d}_{2N}$ the 2-link as shown in Figure 6. The six entries $\mathbf{c}_i^0(1),\ldots,\mathbf{c}_i^0(6)$ of the central jets, defining position, tangent and curvature at the extraordinary point, are initialized as

Figure 5: *The jets of $\mathbf{j}^0$ embedded in 3-space (see also Figure 13).*

$$\mathbf{c}_0^0(1) := \frac{5}{9}\mathbf{d}_0 + \frac{4}{9N}\sum_{j=1}^{N}\mathbf{d}_j, \tag{1}$$

$$\text{For } j=2,\ldots,6, \quad \text{and} \quad \ell := [10,10,9,10-\cos(\frac{2\pi}{N}),9],$$

$$\mathbf{c}_0^0(j) := \frac{\ell(j)}{18}\mathbf{d}_0 + \frac{1}{N}\sum_{k=0}^{N-1}L_k(j,1)\mathbf{d}_k + \frac{1}{N}\sum_{k=0}^{N-1}L_k(j,2)\mathbf{d}_{N+k}.$$

$$\text{For } i=1,\ldots,N-1, \quad \mathbf{c}_i^0 := R^i\mathbf{c}_0^0.$$

The matrices $R\in\mathbb{R}^{6\times 6}$ and $L_k\in^{5\times 2}$ and the initialization of

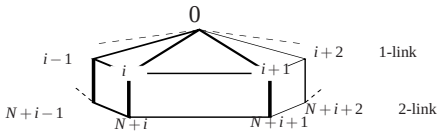

Figure 6: *Indexing the design mesh* $\mathbf{d}$.

the jets $\mathbf{v}_i^0$ and $\mathbf{e}_i^0$ that define the shape at the opposite edge of the triangle are listed in Appendix 6.1. If $N\in\{3,4\}$, the 1-link and the 2-link of the design mesh are each interpreted as a periodic uniform cubic B-spline curve control net. Each is uniformly subdivided to double the valence. This is a standard trick for polar meshes (the adjacent regular mesh need not be refined!) to improve shape without resorting to special rules for low valences [KP06b].

3.3. Local Subdivision Matrix

The local jet control net of the sector at level $m+1$ depends only on the sector at level m via the local subdivision matrix A that does not change with m or sector i (see Figures 7,8):

$$\mathbf{j}_i^{m+1} = A\,\mathbf{j}_i^m, \qquad A\in\mathbb{R}^{27\times 27}.$$

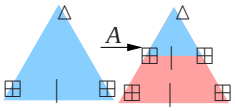

Figure 7: *Local jet refinement conceptually splits each triangle into a smaller triangle and a quadrilateral.*

We choose A so that (i) the refined center jet is determined entirely by the center jet; (ii) the center jet is preserved under binary refinement (by $A_{\triangle,\triangle}$, listed in the Appendix 6.2); (iii) each refined jet $\mathbf{v}_i^{m+1}$ depends only on the central jet (via $A_{\triangle,\boxplus}$) and $\mathbf{v}_i^m$ (via $A_{\boxplus,\boxplus}$); (iv) each refined jet $\mathbf{e}_i^{m+1}$ depends only on the central jet (via $A_{\triangle,|}$) and $\mathbf{e}_i^m$ (via $A_|$). The iconic subscripts hint at the role in mapping old jets to new jets. This yields the simple structure (submatrices listed in Appendix 6.2):

$$A := \begin{bmatrix} A_{\triangle,\triangle} & 0 & 0 & 0 \\ A_{\triangle,\boxplus} & A_{\boxplus,\boxplus} & 0 & 0 \\ A_{\triangle,\boxplus}R & 0 & A_{\boxplus,\boxplus} & 0 \\ A_{\triangle,|} & 0 & 0 & A_| \end{bmatrix}.$$

Choices (i) and (ii) imply that we know the limit jet at the extraordinary point. Two goals determine A in detail: C^2 continuity and changing the surface shape gradually from the boundary of the triangular facets (represented by $\mathbf{v}_i^m$, $\mathbf{v}_{i+1}^m$ and $\mathbf{e}_i^m$) to the central jet $\mathbf{c}_i^m$. The dominant eigenvalues of A are associated with scaling the central jet; the lower eigenvalues with the fading contributions from the boundary.

Theorem 1 The matrix A has a full complement of linearly independent eigenvectors with eigenvalues

$$1,\frac{1}{2},\frac{1}{2},\frac{1}{4},\frac{1}{4},\frac{1}{4},\frac{1}{4},\underbrace{\frac{1}{8},\ldots,\frac{1}{8}}_{7-\text{fold}},\underbrace{\frac{1}{16},\ldots,\frac{1}{16}}_{7-\text{fold}},\underbrace{\frac{1}{32},\ldots,\frac{1}{32}}_{7-\text{fold}}.$$

Proof By (ii) (cf. Appendix 6.2), $A_{\triangle,\triangle}$ has the dominant eigenvalues $1,\frac{1}{2},\frac{1}{2},\frac{1}{4},\frac{1}{4},\frac{1}{4}$. The eigenvalues of $A_|$ are $\frac{1}{8},\frac{1}{16},\frac{1}{32}$ and $A_{\boxplus,\boxplus} = \mathrm{diag}(A_|,A_|,A_|)$. Independence of eigenvectors is checked by explicit eigendecomposition.

4. Representation in Bézier form

To evaluate, we now associate functions with the jets, just as Catmull-Clark subdivision associates one bicubic B-spline with each quadrilateral facet vertex of valence

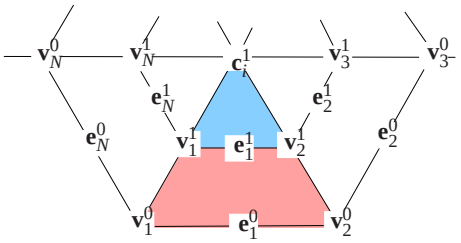

Figure 8: *Jets after one refinement step: the input jets* $\mathbf{v}_i^0$, $\mathbf{c}^0$ *and* $\mathbf{e}_i^0$ *generate a new layer of jets* $\mathbf{v}_i^1$, $\mathbf{e}_i^1$ *and new representations* $\mathbf{c}_i^1$ *of the central jet. Triangular facets are split into a smaller triangular and a quadrilateral facet. The jets associated with the quadrilateral facet define a segment* $\mathbf{x}_i^m$ *of a surface ring* $\mathbf{x}^m$ *(cf. Figure 10).*

four. In fact, the latter has an alternative and equivalent interpretation as jet subdivision: each node and its eight neighbors form a tensor 2-jet $\bar{\mathbf{v}}$ (see Figure 9). Blending the information from four such vertex jets, 4 times 9 degrees of freedom, the Bézier patch $\mathbf{q}$ is in general of degree (5,5). But since the jets overlap and hence contain redundant information, the resulting patch is only of degree (3,3), as expected. In the same spirit, near the extraordinary point, each sector $\mathbf{x}_i^m$, $i \in 0,\ldots,N-1$, of a surface ring is defined by the four vertex jets $\mathbf{v} := [\mathbf{v}_i^{m+1}, \mathbf{v}_{i+1}^{m+1}, \mathbf{v}_i^m, \mathbf{v}_{i+1}^m]$, plus a small perturbation from $\mathbf{e} := [\mathbf{e}_i^m, \mathbf{e}_i^{m+1}]$ as follows (cf. Figure 10) By knot

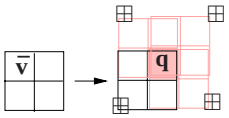

Figure 9: *Bicubic B-spline control net as overlay of four jets of type* $\mathbf{v}$.

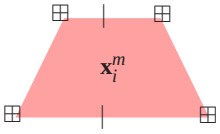

Figure 10: *Jets defining a patch* $\mathbf{x}_i^m$.

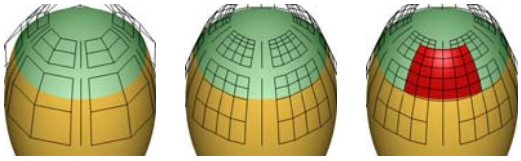

Figure 11: *Conversion of Figure 12 illustrated in 3-space.*

insertion, the four jets $\mathbf{v}$ define the 36 Bézier coefficients of an auxiliary polynomial patch $\mathbf{q}$ (Figures 11, 12). Raising the degree of $\mathbf{q}$ to six in the circular direction and replacing the central column of coefficients by coefficients obtained from jets $\mathbf{e}$ results in a Bézier patch $\mathbf{x}_i^m$ of degree (6,5). The Appendix summarizes the process as a matrix multiplication. The patch can be evaluated by standard algorithms

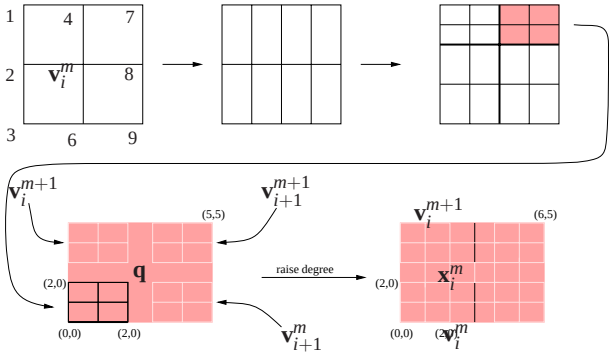

Figure 12: *(top) Conversion of* $\mathbf{v}_i^m$ *by knot insertion to four abutting* 3×3 *blocks of Bézier coefficients (right). (bottom) The upper right block fills as quarter of a* 6×6 *control net of a Bézier patch of degree (5,5).*

and, skipping to a surface ring by eigendecomposition of A [Sta98], yields fast evaluation at arbitrary points.

5. Discussion and Continuity

Implementing jet subdivision is more complex than implementing standard subdivision schemes: compared to standard subdivision there is an additional jet initialization, i.e. one matrix multiplication per design net node (Appendix 6.1); the local subdivision matrix A has about nine times as many entries as standard schemes that work directly on the mesh (Appendix 6.2) and evaluation amounts to applying a more complex linear transformation (Appendix 6.3) than the usual change of basis from B-spline to Bézier representation. Also, because it subdivides polar meshes, the proposed

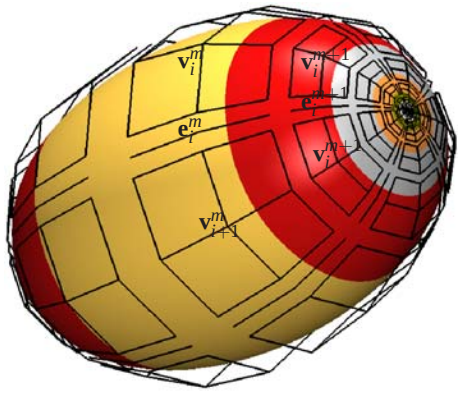

Figure 13: *Summary of the construction: Vertex jets* $\mathbf{v}$ *and edge jets* $\mathbf{e}$ *whose icons* $\boxplus$ *and* $|$ *mimic the representation of the jets as mesh fragments. (Typically, the user will not see or manipulate the jets directly.) The middle, gold surface is of degree (3,3), the other rings* $\mathbf{x}^m$ *are of degree (6,5).*

scheme has a different flavor on quadrilateral and triangular input facets.

However, from the user's point of view, the extra effort and different structure are hidden by the design mesh and the automatic initialization of the jets; and the extra computational and storage effort is negligible since it is confined to extraordinary nodes and, due to sparsity, all formulas reduce to computing products of small matrices and vectors. Therefore, for some applications, the hidden complexity may be an acceptable price to obtain good continuity and shape properties that cannot be obtained by applying few rules with small footprint directly to the design mesh as in standard subdivision. (We derived and optimized the parameters of a number of such direct polar, almost everywhere C^2 subdivision algorithms for comparison.)

To *verify curvature continuity*, we note that adjacent patches $\mathbf{x}_i^m$ and $\mathbf{x}_{i+1}^m$ join C^2 since their transversal derivatives are defined by the same two jets $\mathbf{v}_i^{m-1}$ and $\mathbf{v}_i^m$ by the process just detailed in Section 4. Therefore each ring is C^2. Also due to shared jets, the surface rings $\mathbf{x}^m$ and $\mathbf{x}^{m+1}$ join C^2. In each sector, separately, the eigenvectors of A with eigenvalue 2^{-k} define, by the construction of Section 4, (eigen)functions f_{kj} so that each sector of the surface ring has the expansion

$$\mathbf{x}_i^m = a_0 f_{00} + \frac{1}{2^m}(a_{10} f_{10} + a_{11} f_{11}) + \frac{1}{4^m}(a_{20} f_{20} + a_{21} f_{21} + a_{22} f_{22}) + \sum_{k=3}^{5}\sum_{j=0}^{6} 2^{-km} a_{kj} f_{kj}. \quad (2)$$

In particular, the eigenvectors allow us to choose

$$f_{00} = 1, \quad (f_{10}, f_{11}) = \rho_i, \qquad \{f_{20}, f_{21}, f_{22}\} = \{f_{10}^2, f_{10} f_{11}, f_{11}^2\}, \quad (3)$$

where ρ_i is one sector of the map defined in Appendix 6.4. Abbreviating $(u,v) := 2^{-m}\rho_i(s,t)$ and $g(u,v) := x_i^m(s,t)$, (2) becomes

$$g(u,v) = a_0 + a_{10}u + a_{11}v + a_{20}u^2 + a_{21}uv + a_{22}v^2 + g_3(u,v) + g_4(u,v) + g_5(u,v), \quad (4)$$

where the term g_k corresponds to $\sum_{j=0}^{6} 2^{-km} a_{kj} f_{kj}$, i.e. satisfies $2^{-k} g_k(u,v) = g_k(u/2, v/2)$. Differentiating, we get

$$\partial_u^i \partial_v^j g_k(u/2, v/2) = 2^{-k+i+j} \partial_u^i \partial_v^j g_k(u,v), \quad i+j<3. \quad (5)$$

Therefore the derivatives of $g(u,v)$ have well-defined limits at $(0,0)$. Since the jets $\mathbf{c}_i^0$ consistently define a single unique polynomial of degree two at the extraordinary point, these limits are the same up to second order for all sectors; that is, the surface is C^2.

Note that the third equation of (3) implies that $\mathbf{x}^m$ reproduces ρ^2, a polynomial of degree six in the circular direction. So, while interpolating the jets $\mathbf{v}_i^m$ with patches of degree (5,5) suffices to create a sequence of C^2 joined C^2 rings, we needed to add edge jets in the circular direction for C^2 continuity at the extraordinary point.

Compared to schemes like [Pra97, Rei98], we attribute the observed overall good curvature distribution and shape retention (Figures 16, 17) to the fact that we do not impose a fixed low degree polynomial shape but work with jets. This yields a gradual transition between the main bicubic tensor-product spline body and the extraordinary point, especially for high valences. (Large polar meshes inherit the well-known macroscopic shape of bicubic splines and their pole regions are either less challenging or have less predictable desirable shape than the scenarios in Figure 17.) Compared to Catmull-Clark subdivision, C^2 continuity at the extraordinary point helps the curvature distribution (see Figures 1 and 2). The attenuation of the influence of the outer jets $\mathbf{v}_i^m$ and $\mathbf{e}_i^m$ and dominance of the central jet $\mathbf{c}_i^m$ is controlled by the local subdivision matrix A. This matrix is essentially determined by the requirements (i) through (iv) of Section 3.3 and by the constraints (3). The few remaining degrees of freedom are set to even out the attenuation. Figure 16 illustrates that the twin goals of high smoothness and shape preservation can be achieved simultaneously.

Focus on polar nets made it possible to completely state in print, a specific scheme, the first of its kind. Clearly, there are different choices of local refinement matrices A to be explored, different mesh layouts, patch representations, levels of continuity or number of variables. We must, however, expect that initialization, refinement and change of basis matrices in these scenarios will be more complex.

References

[CNG00] COTRINA NAVAU J., GARCIA N. P.: Modelling surfaces from planar irregular meshes. *Comput. Aided Geom. Design 17*, 1 (2000), 1–15. 2

[GH89] GREGORY J. A., HAHN J. M.: A C^2 polygonal surface patch. *Comp Aided Geom Design 6*, 1 (1989), 69–75. 2

[GH95] GRIMM C. M., HUGHES J. F.: Modeling surfaces of arbitrary topology using manifolds. *Computer Graphics 29*, Annual Conference Series (1995), 359–368. 2

[KP06a] KARČIAUSKAS K., PETERS J.: Guided Subdivision. *Comp Aided Geom Design* (2006). accepted subject to revision. 2

[KP06b] KARČIAUSKAS K., PETERS J.: Surfaces with polar structure. *Computing* (2006), 1–8. to appear, http://www.cise.ufl.edu/research/SurfLab/papers. 1, 3

[KPR04] KARČIAUSKAS K., PETERS J., REIF U.: Shape characterization of subdivision surfaces – Case studies. *Comp. Aided Geom. Design 21*, 6 (2004), 601–614. 1

[Lev06] LEVIN A.: Modified subdivision surfaces with continuous curvature. In *SIGGRAPH, ACM Transactions On Graphics* (2006), p. to appear. 2

[LL03] LEVIN A., LEVIN D.: Analysis of quasi-uniform subdivision. *Appl Comp Harm Anal*, 15 (2003), 18–32. 2

[Loo04] LOOP C.: Second order smoothness over extraordinary vertices. In *Symp Geom Processing* (2004), pp. 169–178. 2

[MWW01] MORIN G., WARREN J. D., WEIMER H.: A subdivision scheme for surfaces of revolution. *Comp Aided Geom Design 18*, 5 (2001), 483–502. 2

[Pet02] PETERS J.: C^2 free-form surfaces of degree (3,5). *Comp Aided Geom Design 19*, 2 (2002), 113–126. 2

[Pra97] PRAUTZSCH H.: Freeform splines. *Comput. Aided Geom. Design 14*, 3 (1997), 201–206. 2, 5

[PU98] PRAUTZSCH H., UMLAUF G.: Improved triangular subdivision schemes. In *Computer Graphics International* (1998), pp. 626–632. 2

[Rei98] REIF U.: TURBS—topologically unrestricted rational *B*-splines. *Constr. Appr. 14*, 1 (1998), 57–77. 2, 5

[RP05] REIF U., PETERS J.: Topics in multivariate approximation and interpolation. In *Structural Analysis of Subdivision Surfaces – A Summary* (2005), et al. K. J., (Ed.), pp. 149–190. 2

[SD05] SABIN M., DODGSON N.: A circle-preserving variant of the four-point subdivision scheme. In *Mathematical Methods for Curves and Surfaces: Tromso 2004* (2005), Daehlen M., Schumaker, (Eds.), Nashboro Press, pp. 275–286. 2

[Sta98] STAM J.: Exact evaluation of Catmull-Clark subdivision surfaces at arbitrary parameter values. In *SIGGRAPH* (1998), pp. 395–404. 4

[SW05] SCHAEFER S., WARREN J. D.: On C^2 triangle/quad subdivision. *ACM Trans. Graph 24*, 1 (2005), 28–36. 2

[WW02] WARREN J., WEIMER H.: *Subdivision Methods for Geometric Design*. Morgan Kaufmann Publishers, 2002. 2

[XYD06] XUE Y., YU T. P.-Y., DUCHAMP T.: Jet subdivision schemes on the *k*-regular complex. *Comp Aided Geom Design* (2006). to appear. 2

[YZ04] YING L., ZORIN D.: A simple manifold-based construction of surfaces of arbitrary smoothness. *ACM TOG 23*, 3 (Aug. 2004), 271–275. 2

[ZLLT06] ZULTI A., LEVIN A., LEVIN D., TEICHER M.: C^2 subdivision over triangulations with one extraordinary point. *Comp Aided Geom Design 23*, 2 (feb 2006), 157–178. 2

[ZS00] ZORIN D., SCHRÖDER P. (Eds.):. *Subdivision for Modeling and Animation* (2000), Course Notes, ACM SIGGRAPH. 2

6. Appendix

This appendix contains three sparse matrices, broken into small pieces to allow easy implementation of the algorithm. The first matrix (Section 6.1) initializes the jets and has pieces L_k, L_e, L_v and R. The second matrix, A refines the local jets at each subdivision step (Section 6.2). The third matrix, K, converts jets to polynomial pieces in Bézier form (Section 6.3).

Throughout, the sector indices $i = 1,\dots,N$, are counted modulo the valence N. We abbreviate $\mathsf{c} := \cos(\frac{2\pi}{N})$. diag(vector) is the diagonal matrix with diagonal 'vector', and $A(:, i:j)$ denotes columns i through j of a matrix A.

6.1. Jet Initialization matrix

With the indexing of the design mesh $\mathbf{d}$ as in Figure 6,

$$\mathbf{v}_i^0 := L_v \mathbf{d}_v, \qquad \mathbf{e}_i^0 := L_e \mathbf{d}_e,$$

where

$$\mathbf{d}_v := [\mathbf{d}_0, \mathbf{d}_{i-1}, \mathbf{d}_{N+i-1}, \mathbf{d}_i, \mathbf{d}_{N+i}, \mathbf{d}_{i+1}, \mathbf{d}_{N+i+1}],$$
$$\mathbf{d}_e := [\mathbf{d}_v, \mathbf{d}_{i+2}, \mathbf{d}_{N+i+2}].$$

$$L_v := \frac{1}{14400}\begin{bmatrix} 4020 & 3850 & 475 & 5236 & 646 & 154 & 19 \\ 1320 & 4300 & 1150 & 5848 & 1564 & 172 & 46 \\ 240 & 3400 & 2500 & 4624 & 3400 & 136 & 100 \\ 4020 & 1078 & 133 & 7084 & 874 & 1078 & 133 \\ 1320 & 1204 & 322 & 7912 & 2116 & 1204 & 322 \\ 240 & 952 & 700 & 6256 & 4600 & 952 & 700 \\ 4020 & 154 & 19 & 5236 & 646 & 3850 & 475 \\ 1320 & 172 & 46 & 5848 & 1564 & 4300 & 1150 \\ 240 & 136 & 100 & 4624 & 3400 & 3400 & 2500 \end{bmatrix},$$

$$L_e := \frac{1}{28800}\begin{bmatrix} 8040 & 154 & 19 & 9086 & 1121 & 9086 & 1121 & 154 & 19 \\ 2640 & 172 & 46 & 10148 & 2714 & 10148 & 2714 & 172 & 46 \\ 480 & 136 & 100 & 8024 & 5900 & 8024 & 5900 & 136 & 100 \end{bmatrix}.$$

The matrix L_k for initializing the central jet $\mathbf{c}_0^0$,

$$L_k := \begin{bmatrix} w_1 c_k + \frac{4}{9} & w_9 c_k \\ w_1 c_{k-1} + \frac{4}{9} & w_9 c_{k-1} \\ w_2 c_k^2 + 2 w_1 c_k - w_3 & 4 w_5 c_k^2 + 2 w_9 c_k + w_6 \\ w_2 c_k c_{k-1} + w_1 (c_k + c_{k-1}) - w_4 & 4 w_5 c_k c_{k-1} + w_9 (c_k + c_{k-1}) + w_6 \mathsf{c} \\ w_2 c_k c_{k-2} + 2 w_1 c_{k-1} + w_7 & 4 w_5 c_k c_{k-2} + 2 w_9 c_{k-1} + w_8 \end{bmatrix},$$

depends on k via $c_k := \cos(\frac{2\pi k}{N})$ and

$$w_1 := \frac{11}{81}(2+\mathsf{c}), \quad w_9 := \frac{-w_1}{110}, \quad w_2 := \frac{88}{81}\mathsf{c}^2 - \frac{56}{135}\mathsf{c} + \frac{136}{405},$$
$$w_3 := \frac{44}{81}\mathsf{c}^2 - \frac{28}{135}\mathsf{c} - \frac{659}{2025}, \quad w_4 := w_3 \mathsf{c} + \frac{4}{9}(\mathsf{c}-1),$$
$$w_5 := -\frac{1}{405}\mathsf{c}^2 + \frac{1}{135}\mathsf{c} + \frac{1}{405}, \quad w_6 := \frac{2}{405}\mathsf{c}^2 - \frac{2}{135}\mathsf{c} + \frac{7}{4050},$$
$$w_7 := -2 w_3 \mathsf{c}^2 - \frac{898}{2025}\mathsf{c}^2 - \frac{28}{135}\mathsf{c} + \frac{1339}{2025},$$
$$w_8 := \frac{4}{405}\mathsf{c}^4 - \frac{4}{135}\mathsf{c}^3 - \frac{2}{135}\mathsf{c}^2 + \frac{2}{135}\mathsf{c} + \frac{47}{4050}.$$

The matrix

$$R := \begin{bmatrix} 1 & 0 & 0 & 0 & 0 & 0 \\ 0 & 0 & 1 & 0 & 0 & 0 \\ 2(1-\mathsf{c}) & -1 & 2\mathsf{c} & 0 & 0 & 0 \\ 0 & 0 & 0 & 0 & 0 & 1 \\ 0 & 0 & 2(1-\mathsf{c}) & 0 & -1 & 2\mathsf{c} \\ 4(1-\mathsf{c})^2 & -4(1-\mathsf{c}) & 8(1-\mathsf{c})\mathsf{c} & 1 & -4\mathsf{c} & 4\mathsf{c}^2 \end{bmatrix} \qquad (6)$$

encodes C^2 constraints between the central jets $\mathbf{c}_i^0$.

6.2. The local subdivision matrix A

The submatrixes of the local subdivision matrix $A \in \mathbb{R}^{27\times 27}$ that maps $\mathbf{j}_i^{m+1} = A\,\mathbf{j}_i^m$ are $A_{\triangle,\triangle}$,$A_{|}$, $A_{\boxplus,\boxplus}$, $A_{\triangle,\boxplus}$, $A_{\triangle,|}$ where the iconic subscripts hint at the role in mapping old jets to new jets.

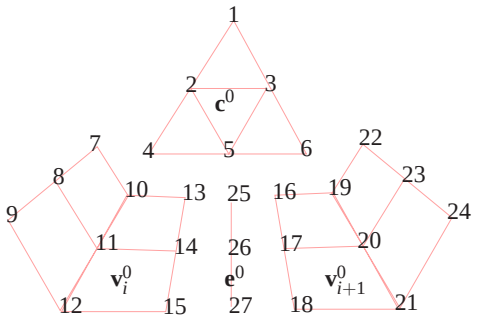

Figure 14: *Indexing of local jet representations in vector* $\mathbf{j}$. *For example,* $\mathbf{j}_{i-1}^m(16:24) = \mathbf{v}_i^m = \mathbf{j}_i^m(7:15)$.

$$A_{\triangle,\triangle} := \frac{1}{4}\begin{bmatrix} 4&0&0&0&0&0\\ 2&2&0&0&0&0\\ 2&0&2&0&0&0\\ 1&2&0&1&0&0\\ 1&1&1&0&1&0\\ 1&0&2&0&0&1\end{bmatrix}, \qquad A_{|} := \frac{1}{576}\begin{bmatrix} 278&-109&11\\ 488&-160&14\\ 608&-112&8\end{bmatrix},$$

$$A_{\boxplus,\boxplus} := \operatorname{diag}(A_{|},A_{|},A_{|}),$$

$$A_{\triangle,\boxplus}(:,1) := 1 - \sum_{j=2}^{6} A_{\triangle,\boxplus}(:,j) - \sum_{j=7}^{16} A_{\boxplus,\boxplus}(:,j),$$

$$k_0 := 28 - 2\mathsf{c} + \mathsf{c}^2\ ,\ k_1 := 8 + \mathsf{c}\ ,\ k_2 := 8 + 7\mathsf{c}\ ,$$

$$k_3 := 28 + 94\mathsf{c} + 49\mathsf{c}^2\ ,\ k_4 := 52 + 34\mathsf{c} - 5\mathsf{c}^2\ ,$$

$$A_{\triangle,\boxplus}(:,2:6) := \frac{1}{1280(2+\mathsf{c})^2}\operatorname{diag}(1,4,16,1,4,16,1,4,16)\cdot\ldots$$

$$\ldots\begin{bmatrix} 3(1294{+}553\mathsf{c}{-}461\mathsf{c}^2) & -108(15{-}4\mathsf{c}) & 46k_3 & -276k_2 & 414\\ 27(26{+}3\mathsf{c}{-}15\mathsf{c}^2) & -36(7{-}4\mathsf{c}) & 10k_3 & -60k_2 & 90\\ 12(1{-}\mathsf{c})(5{+}4\mathsf{c}) & -18(1{-}\mathsf{c}) & k_3 & -6k_2 & 9\\ 3(322{+}223\mathsf{c}{+}445\mathsf{c}^2) & 828(1{-}\mathsf{c}) & 46k_4 & 828\mathsf{c} & -414\\ 9(2{-}\mathsf{c}{+}29\mathsf{c}^2) & 180(1{-}\mathsf{c}) & 10k_4 & 180\mathsf{c} & -90\\ -12(1{-}\mathsf{c})(1{+}2\mathsf{c}) & 18(1{-}\mathsf{c}) & k_4 & 18\mathsf{c} & -9\\ -3(178{-}761\mathsf{c}{-}11\mathsf{c}^2) & -36(1{-}34\mathsf{c}) & 46k_0 & 276k_1 & 414\\ -3(86{-}139\mathsf{c}{-}\mathsf{c}^2) & -108(1{-}2\mathsf{c}) & 10k_0 & 60k_1 & 90\\ -36(1{-}\mathsf{c}) & -18(1{-}\mathsf{c}) & k_0 & 6k_1 & 9\end{bmatrix}.$$

With $\ell_0 := -190 + 1169\mathsf{c} + 11\mathsf{c}^2$,

$$\ell_1 := -122 + 211\mathsf{c} + \mathsf{c}^2\ ,\ \ell_2 := 49 + 4\mathsf{c} + \mathsf{c}^2\ ,$$

$$A_{\triangle,|}(:,1) := 1 - \sum_{j=2}^{6} A_{\triangle,|}(:,j) - \sum_{j=1}^{3} A_{|}(:,j)$$

$$A_{\triangle,|}(:,2:6) := \frac{1}{2560(2+\mathsf{c})^2}\operatorname{diag}(1,4,32)\cdot\ldots$$

$$\ldots\begin{bmatrix} 3\ell_0 & 3\ell_0 & 1656 & 92\ell_2 & 1656\\ 3\ell_1 & 3\ell_1 & 360 & 20\ell_2 & 360\\ -27(1-\mathsf{c}) & -27(1-\mathsf{c}) & 18 & \ell_2 & 18\end{bmatrix}.$$

6.3. The change of basis operator

The lower left nine Bézier coefficients of the auxiliary patch $\mathbf{q}$ of degree (5,5) representing four vertex jets $\mathbf{v}_i^m$ are, by knot insertion,

$$\begin{bmatrix}\mathbf{q}(0,2) & \mathbf{q}(1,2) & \mathbf{q}(2,2)\\ \mathbf{q}(0,1) & \mathbf{q}(1,1) & \mathbf{q}(2,1)\\ \mathbf{q}(0,0) & \mathbf{q}(1,0) & \mathbf{q}(2,0)\end{bmatrix} = \mathbf{q}(0:2,0:2) := K\mathbf{v}_i^m \qquad K := \frac{1}{36}\begin{bmatrix} 4&4&1&8&8&8&4&4&1\\ 0&0&0&8&8&2&8&8&2\\ 0&0&0&0&0&0&16&16&4\\ 6&3&0&12&6&0&6&3&0\\ 0&0&0&12&6&0&12&6&0\\ 0&0&0&0&0&0&24&12&0\\ 9&0&0&18&0&0&9&0&0\\ 0&0&0&18&0&0&18&0&0\\ 0&0&0&0&0&0&36&0&0\end{bmatrix}.$$

Here, the entries of $\mathbf{v}_i^m$ are in their order as in Figure 12, *left*, i.e. $\mathbf{v}_i^m(\begin{bmatrix}1&4&7\\2&5&8\\3&6&9\end{bmatrix})$. The matrix K can also be used to generate the remaining entries of $\mathbf{q}$ by applying the straightforward symmetries of the indices of $\mathbf{q}$ and the jets:

$$\mathbf{q}(0:2,5:3) \leftarrow \mathbf{v}_i^{m+1}(\begin{bmatrix}3&6&9\\2&5&8\\1&4&7\end{bmatrix}),\quad \mathbf{q}(5:3,5:3) \leftarrow \mathbf{v}_{i+1}^{m+1}(\begin{bmatrix}9&6&3\\8&5&2\\7&4&1\end{bmatrix}),$$
$$\mathbf{q}(0:2,0:2) \leftarrow \mathbf{v}_i^{m}(\begin{bmatrix}1&4&7\\2&5&8\\3&6&9\end{bmatrix}),\quad \mathbf{q}(5:3,0:2) \leftarrow \mathbf{v}_{i+1}^{m}(\begin{bmatrix}7&4&1\\8&5&2\\9&6&3\end{bmatrix}).$$

After raising the degree of $\mathbf{q}$ to six in the circular direction and renaming it $\mathbf{x}_i^m$, we replace the central column of coefficients by

$$\mathbf{x}_i^m(3,0:2) = \frac{1}{9}\begin{bmatrix}4&4&1\\6&3&0\\9&0&0\end{bmatrix}\mathbf{e}_i^m, \qquad \mathbf{x}_i^m(3,3:5) = \frac{1}{9}\begin{bmatrix}0&0&9\\0&6&3\\4&4&1\end{bmatrix}\mathbf{e}_i^{m+1},$$

where the three entries of $\mathbf{e}_i^m$ are indexed, in the natural order, i.e. as $\begin{bmatrix}1\\2\\3\end{bmatrix}$.

6.4. The map ρ

The map

$$\rho : [0,1]^2 \times \{1,\ldots,N\} \to \mathbb{R}^2$$

is a C^2 spline ring of piecewise degree (3,1). Its outer and inner layers differ by a scaling factor $1/2$, $\rho_{1i} := 2\rho_{0i}$ where

$$\rho_{0i} := \begin{bmatrix}\cos(i\alpha)\\ \sin(i\alpha)\end{bmatrix}, \quad \alpha := \frac{2\pi}{N}.$$

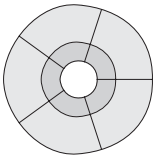

Figure 15: *The maps* ρ *and* $\rho/2$ *for* $N = 5$.

and each represents a periodic planar uniform cubic spline. We note that ρ is regular and injective and ρ and $\rho/2$ join C^2 (see Figure 15), tesselating the plane with common center.

Acknowledgements The presentation benefited from the helpful feedback of the reviewers. The work was supported by NSF Grants DMI-0400214 and CCF-0430891.

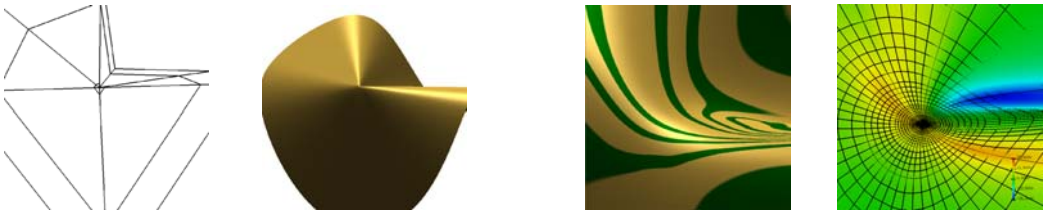

Figure 16: *A semisharp curvature continuous blend attests to the ability of polar guided subdivision to both preserve* macroscopic shape *and local* curvature continuity. *Note the small design mesh triangles at the center, intended to force a rapid transition near the extraordinary node. The right figures show reflection lines and mean curvature at the enlarged center.*

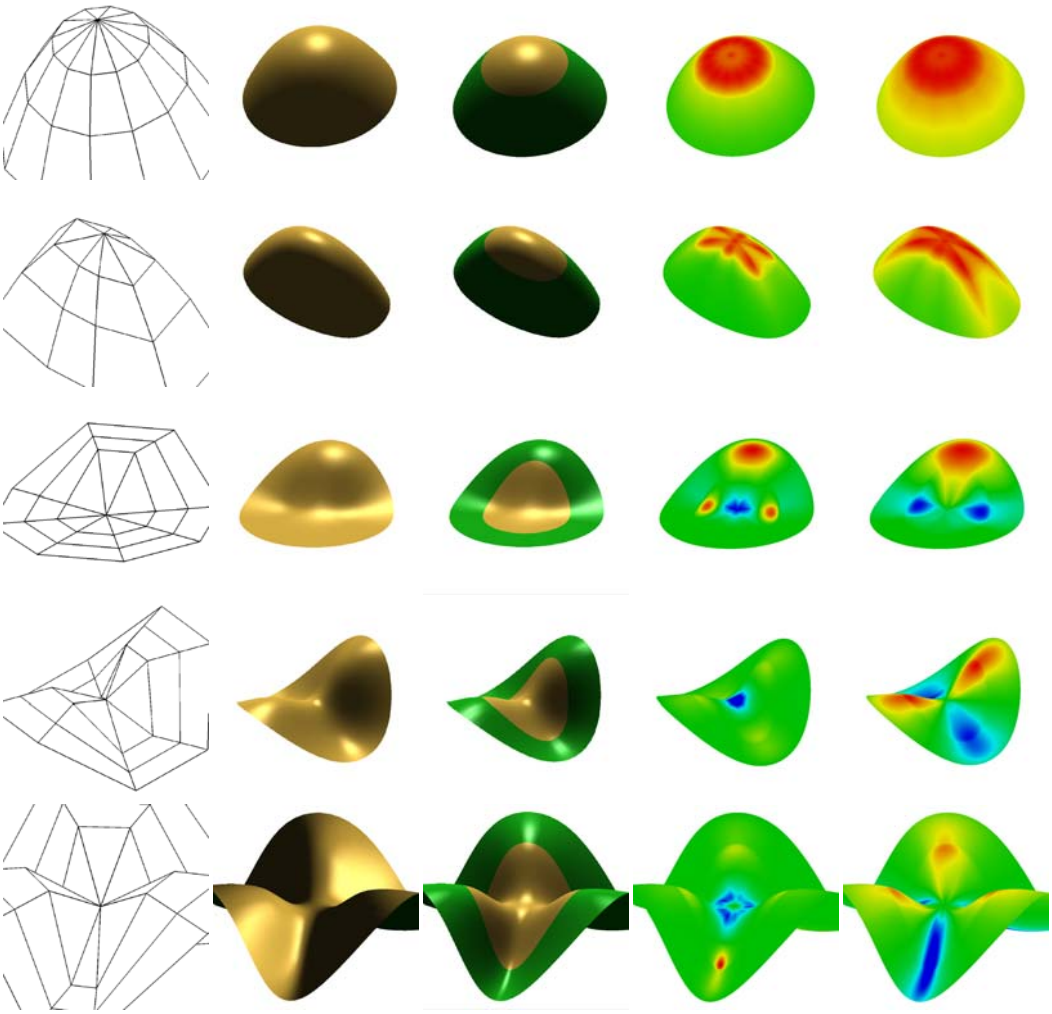

Figure 17: *Shape and smoothness analysis of the neighborhood of an extraordinary point. (top to bottom) basic cone, elongated cone, saddle, single ridge, monkey saddle, (left to right) control net, shape, patches of degree (3,3) shaded green, Gauss curvature and mean curvature texture centered at 0=green.*